

https://doi.org/10.1070/QEL16289

Supercontinuum spectrum upon filamentation of laser pulses under conditions of strong and weak anomalous group velocity dispersion in transparent dielectrics

S.V. Chekalin, V.O. Kompanets, A.E. Dormidonov, E.D. Zaloznaya, V.P. Kandidov

Abstract. **Using experiment and numerical simulation, we study the effect of anomalous group velocity dispersion (AGVD) on the formation of a visible supercontinuum band and light bullets arising in the course of filamentation of mid-IR femtosecond pulses in fused silica and fluorides. It is found that the anti-Stokes shift of the visible band increases with increasing energy of the pulse, the centre wavelength of which lies in the region of weak AGVD, and does not depend on this energy in the region of strong AGVD. A criterion is introduced for assessment of the AGVD 'strength', at which the stable visible supercontinuum band accompanies the formation of a robust light bullet in the mid-IR filament.**

Keywords: *filamentation, femtosecond pulses, light bullet, supercontinuum, anomalous group velocity dispersion.*

1. Introduction

Filamentation of a femtosecond laser pulse in dielectrics is accompanied by the generation of a supercontinuum (SC), for which the spectral band extends from the UV-to-mid-IR range [1, 2]. The supercontinuum with the broadest band (a few octaves) is generated during the pulse filamentation under the conditions of anomalous group velocity dispersion (AGVD) [3–6]. In this case, an isolated wing is formed in the visible range of the SC, the spectral bandwidth of which becomes narrower with the maximum shifted towards the anti-Stokes region, when the centre wavelength λ_0 of the incident light is increased [7–11].

The physical origin of the broad spectral minimum that arises between the anti-Stokes wing and the region of the pulse centre wavelength is reproduced by the interference model [12] that allows the analytical calculation of the SC frequency-angular spectrum, as well as by the allied three-wave mixing model [13] that describes the formation of the global maximum in the frequency-angular spectrum.

The generation of a broadband SC and its anti-Stokes wing in the case of AGVD is closely related to the spatiotemporal self-compression of laser radiation and the formation of high-intensity light bullets (LBs), the duration of which can amount to less than two optical oscillations [14–16]. A LB is a robust object, and in the course of the formation of a train of LBs in a near-IR filament, each bullet 'expels' in the visible range of the SC a similar portion of energy, the amount of which decreases with increasing pulse wavelength [17, 18].

The effect of AGVD on the formation of the SC and LB under femtosecond filamentation depends on the centre wavelength of the incident pulse and the material dispersion of the medium. We found [19] the general rule that determines the dispersion shift of the anti-Stokes band of the LB supercontinuum, which is confirmed by the spectroscopic studies of the pulse filamentation in the near- and mid-IR range in fused silica and fluorides. To date, a number of experiments have been carried out on the filamentation of pulses at the wavelength that falls in the region of zero group velocity dispersion. In Ref. [20] it is shown that for the close-to-zero AGVD, the filament in the BK 7 glass has a maximal length, and the spectral width of the SC approaches 650 nm and covers the region having the width of the order of the pulse wavelength. According to the experiments carried out in sapphire and fused silica [21], a femtosecond pulse under the conditions of weak AGVD filamentation decays into subpulses, its spectrum consisting of two maxima near the initial wavelength. On the contrary, under the conditions of moderate or strong AGVD, the pulse becomes compressed and the LB with a broad SC spectrum is formed. From the numerical simulation [22] it follows that at the pulse power exceeding by three times the critical self-focusing power P_{cr}, a single LB is formed in the filament, when the dispersion length is much greater than the self-focusing length, and a sequence of LBs is formed for the close values of dispersion and diffraction lengths.

In the present paper, we study the visible band of the SC spectrum and the LB formation in the process of femtosecond pulse filamentation at a number of wavelengths in the regions of weak and strong AGVD in fused silica, BaF_2, and CaF_2. The regime of single filamentation at the pulse power exceeding P_{cr} by 1.2–3 times is considered. We analyse the role of the pulse energy in the formation of the SC visible band and LB in the regions of weak and strong AGVD. Based on the experimental and numerical results, we show that the ratio of dispersion and diffraction lengths is a similarity criterion that determines the AGVD 'strength', providing the formation of the LB with a stable SC visible-range band in the filament.

2. Experiment

The experimental studies of the SC spectrum were carried out using the spectrometric femtosecond system based on a TOPAS tunable parametric amplifier, combined with a

S.V. Chekalin, V.O. Kompanets Institute of Spectroscopy, Russian Academy of Sciences, ul. Fizicheskaya 5, Troitsk, 108840 Moscow, Russia; e-mail: chekalin@isan.troitsk.ru, kompanetsvo@isan.troitsk.ru;
A.E. Dormidonov, E.D. Zaloznaya, V.P. Kandidov Department of Physics, M.V. Lomonosov Moscow State University, Vorob'evy Gory, 119992 Moscow, Russia;
e-mail: dormidonov@gmail.com, kandidov@physics.msu.ru

Received 19 December 2016
Kvantovaya Elektronika **47** (3) 252–258 (2017)
Translated by V.L. Derbov

Spitfire Pro regenerative amplifier. The centre wavelength of laser pulses varied from 1400 to 3800 nm, which corresponds to the regions of weak and strong AGVD of the materials in question. The pulse energy W was measured using a Fieldmax meter with a PS-10 detector. For implementing the single-filament regime we varied W within the range $W = (1-15) \times 10^{-6}$ J. For the signal wave of the parametric amplifier at $\lambda_0 =$ 1400 nm the duration of the pulses at the half-maximum level $t_{0.5}$ amounted to $t_{0.5} = 70$ fs, the diameter of the output beam being $d_{0.5} = 1.7$ mm. For the idler wave at $\lambda_0 = 2600$ nm the pulse duration $t_{0.5}$ increased to 100 fs, and the output beam had an elliptic cross section, 1.7 × 2.4 mm. At $\lambda_0 = 3800$ nm the pulse duration was $t_{0.5} = 100$ fs, the cross section of the beam having the size 2.5 × 3.8 mm. The pulses were focused on the input face of the samples by means of a thin silica lens with a focal length $F = 19$ cm in the near-IR and $F = 21$ cm in the mid-IR range. The spectra were recorded using an ASP-100MF fibre spectrometer and an ASPIRHS spectrometer (Avesta Ltd) in the spectral ranges 200–1100 nm and 1200–2600 nm, respectively. To obtain the anti-Stokes band spectra, the diverging SC radiation was focused onto a thin diffuse scatterer, placed immediately before the spectrometers. The spectra were studied in the regime of single filamentation, in which the peak pulse power in all materials amounted to $(1.2-4.0)P_{cr}$.

Under the weak AGVD conditions, the filamentation was implemented using the pulses at the wavelength, insignificantly exceeding the wavelength $\lambda_{k_2=0}$, at which the parameter $k_2 = \partial^2 k(\omega)/\partial\omega^2$ that determines the group velocity dispersion (GVD) turns into zero. In fused silica, $\lambda_{k_2=0} = 1273$ nm, in the CaF_2 crystal, $\lambda_{k_2=0} = 1546$ nm, and in BaF_2, $\lambda_{k_2=0} = 1925$ nm [23]. The spectra in the anti-Stokes region were studied in fused silica under the filamentation of pulses at the wavelength $\lambda_0 = 1400$ nm, at which $k_2 = -11.7$ fs^2 mm^{-1} and $P_{cr} =$ 8.2 MW. The corresponding parameters were $\lambda_0 = 1800$ nm, $k_2 = -10.9$ fs^2 mm^{-1}, $P_{cr} = 18.0$ MW for CaF_2 and $\lambda_0 =$ 2100 nm, $k_2 = -5.9$ fs^2 mm^{-1}, $P_{cr} = 15.7$ MW for BaF_2, respectively. It was found that under the conditions of weak AGVD the spectrum of the anti-Stokes SC band essentially shifts towards the short-wavelength region with the growth of the pulse energy (Fig. 1a). In the process of filamentation in fused silica, CaF_2, and BaF_2, the maximum of spectral intensity in the anti-Stokes band λ^{as}_{max} shifts from the IR region 800–1000 nm to the visible region 600–500 nm, when the pulse energy is increased approximately by 30%.

Under the conditions of strong AGVD, when the magnitude of the parameter k_2 increases by more than ten times ($k_2 = -285$ fs^2 mm^{-1}, $P_{cr} = 28$ MW at $\lambda_0 = 2600$ nm in fused silica, $k_2 = -115$ fs^2 mm^{-1}, $P_{cr} = 52$ MW at $\lambda_0 = 3060$ nm in CaF_2, $k_2 = -112$ fs^2 mm^{-1}, $P_{cr} = 51.5$ MW at $\lambda_0 = 3750$ nm in BaF_2), in all materials the spectral position of the anti-Stokes band maximum λ^{as}_{max} is independent of the pulse energy W, varied within the range, corresponding to the single filamentation regime (Fig. 1b).

3. Numerical modelling

To analyse the observed features of the SC spectrum formation we performed numerical modelling of the pulse filamentation with the parameters, close to the experimental ones. We used the approximation of a slowly varying envelope [24], the equations of which include the nonstationary variations in the medium refractive index induced by the Kerr and plasma nonlinearity, the diffraction of radiation, the medium material dispersion, described by the Sellmeier formula, the effect of the pulse front self-steepening, the laser plasma generation due to photoionisation and avalanche ionisation of dielectrics, as well as the radiation attenuation caused by inverse bremsstrahlung and photoionisation losses. The complete system of multidimensional nonlinear equations with the dimensionality 3D + 1 that describes the spatiotemporal transformation of the wave packet envelope and the generation of a laser plasma in the medium is presented in detail in Refs [18, 25]. The radiation at the input face of the sample was specified in the form of a collimated beam of transform-limited pulsed radiation having a Gaussian spatiotemporal shape

$$A(r,t,z=0) = A_0 \exp\left(-\frac{r^2}{2a_0^2} - \frac{t^2}{2\tau_0^2}\right), \quad (1)$$

where a_0 and τ_0 are the beam radius and the pulse half-duration at the intensity level e^{-1}; and A_0 is the peak amplitude of the light field. The parameter τ_0 is related to the measured pulse duration $t_{0.5}$ as $t_{0.5} = 2\sqrt{\ln 2}\,\tau_0$. The radius a_0 of the beam, focused at the input face of the sample by means of a lens having a focal length F, was estimated using the formula $a_0 = F\lambda_0\sqrt{\ln 2}/(\pi d_{0.5})$, where $d_{0.5}$ is the beam diameter at the lens. The amplitude A_0 was determined using the peak radiation intensity $I_0 = c_0 n_0 \varepsilon_0 A_0^2/2$, where $\varepsilon_0 = 8.85 \times 10^{-12}$ F m^{-1} is the electric constant; n_0 is the refractive index of the medium; and c_0 is the velocity of light. The peak values of the intensity I_0 and the power $P_0 = \pi a_0^2 I_0$ of the incident pulse were calculated from the measured values of the pulse energy $W = \sqrt{\pi} \times \tau_0 P_0$.

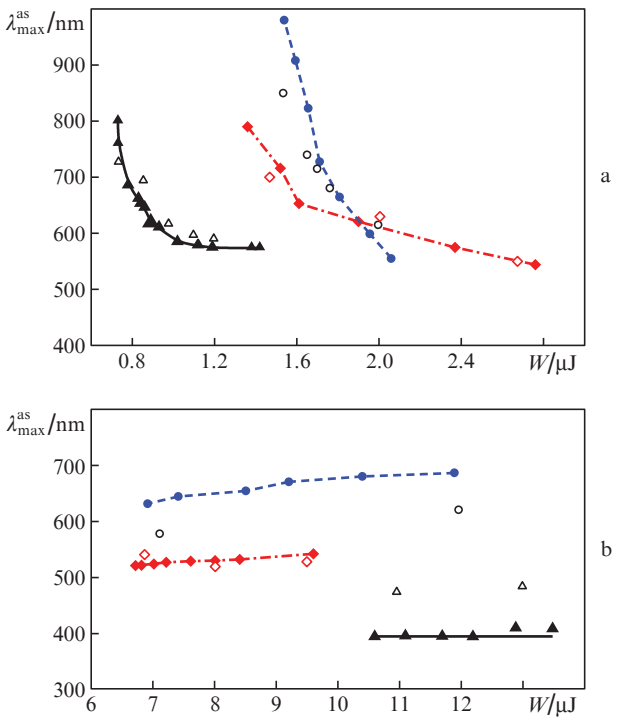

Figure 1. Dependences of the wavelength λ^{as}_{max} of the visible SC band spectral maximum on the pulse energy for the filamentation in (▲, △) fused silica, (◆, ◇) CaF_2 and (●, ○) BaF_2 under the conditions of (a) weak and (b) strong AGVD; filled points present the experiment and empty ones present the numerical simulation.

3.1. Weak AGVD

For fused silica we considered the radiation at the wavelength $\lambda_0 = 1400$ nm with $\tau_0 = 42$ fs, $a_0 = 41.5$ μm (Table 1). The dispersion length of the considered wave packet $L_{dis} = \tau_0^2/|k_2| =$ 152 mm exceeds its diffraction length $L_{dif} = ka_0^2 = 11$ mm by more than an order of magnitude. Figure 2 presents the spatial variations in the pulse axial intensity distribution $I(t, r = 0, z)$ and concentration of electrons $N_e(r = 0, z)$ for the nonlinearity parameters $R = P_0/P_{cr} = 1.2$ and $R = 2.0$ in the local reference frame moving with the pulse, $\tau = t - z/v_g$, where v_g is the group velocity of the pulse.

At a low energy ($R = 1.2$), the peak intensity I_{peak} and the concentration of electrons $N_e(r = 0, z)$ at the axis smoothly increase, reaching a maximum in the nonlinear focus at the distance $z = 14.0$ mm (Fig. 2a). The pulse duration at the axis of the wave packet monotonically decreases along the filament, reaching a minimum in the nonlinear focus, and then grows again. The difference of the formed wave packet propagation velocity v_b from the group velocity v_g of the initial pulse at $R = 1.2$ is not large: $\Delta v = v_g - v_b = 0.0016v_g$.

For the pulse with a higher energy ($R = 2$) the peak intensity I_{peak} varies nonmonotonically with the distance (Fig. 2b). At first I_{peak} increases due to self-focusing of the most high-power layers of the pulse, shifted towards its tail because of the nonlinear response delay, forming a local maximum at the distance $z = 6.8$ mm. Then, I_{peak} decreases due to the diffraction and plasma defocusing, and then increases again due to the temporal compression of the wave packet under AGVD, achieving a global maximum at $z = 7.1$ mm. The compression in time is more efficient, which is confirmed by a smaller duration of the second maximum. The velocity difference Δv between v_g and the wave packet velocity v_b at $R = 2$ becomes more essential and amounts to $0.002v_g$. An increase in the pulse energy also causes the reduction of the distance at which the plasma appears, and the length of the plasma channel, in which the concentration of electrons $N_e > 10^{-4}N_0$ (N_0 being the concentration of neutral particles) increases from 0.15 to 0.50 mm. The minimal duration at the wave packet axis is close to one period of the light field.

The process of pulse compression in the course of filamentation is illustrated by the greyscale patterns of the intensity spatiotemporal distribution $\lg(I(r, t)/I_0)$ in the LB and the axial intensity profiles $I(r = 0, t)$ at $R = 1.2$ (Fig. 3a) and $R = 2$ (Fig. 3b) at a number of characteristic distances. The left-hand panels with the distributions $\lg(I(r, t)/I_0)$ in Fig. 3 correspond to the appearance of a laser plasma in the filament, the central panels correspond to the achievement of the maximal peak intensity I_{peak} in the wave packet, and the right-hand panels correspond to the maximal localisation of the SC anti-Stokes wing spectrum. One can see that independent of the pulse energy, the plasma generation causes the aberrational defocusing and the formation of ring patterns in the tail of the wave packet. For the pulse having a greater energy, the self-phase modulation is stronger, and the formation of the second maximum begins at the leading edge of the pulse, causing no formation of the second LB in the case of weak AGVD (Fig. 3b). With an increase in the pulse energy W the maximal value of the peak intensity I_{peak} increases from 48 to 61 TW cm^{-2}.

The formation of the anti-Stokes SC wing in the course of pulse propagation under the conditions of weak AGVD is illustrated by Fig. 4, demonstrating the pulse spectrum in the logarithmic scale $\lg[S(\lambda)/S(\lambda_0)]$, where $S(\lambda_0)$ is the spectral intensity at the wavelength of the incident pulse. The spectra are presented at the same distances, as the intensity distributions $I(r, t)$. In the beginning of the filament the SC spectrum is homogeneously broadened, and then the isolated anti-Stokes wing is formed, in which the spectral intensity maximum exceeds $0.01S(\lambda_0)$. The spectral intensity in the region that separates the band near the carrier wavelength λ_0 from the anti-Stokes wing, is smaller than $S(\lambda_0)$ by a few orders of magnitude. This region is formed by destructive interference of broadband SC radiation, generated due to the self-phase modulation at the trailing edge of the pulse under the condi-

Table 1. Parameters of pulses in the case of weak AGVD.

Medium	λ_0/nm	τ_0/fs	a_0/μm	W/μJ	R	L_{dif}/mm	L_{dis}/mm	L_{dis}/L_{dif}
Fused silica	1400	42	41	0.7–1.4	1.2–2.4	11	152	14
BaF_2	2100	42	46	1.5–2.1	1.3–1.8	9.3	300	32
CaF_2	1800	42	41	1.5–2.7	1.1–2.0	8.4	170	20

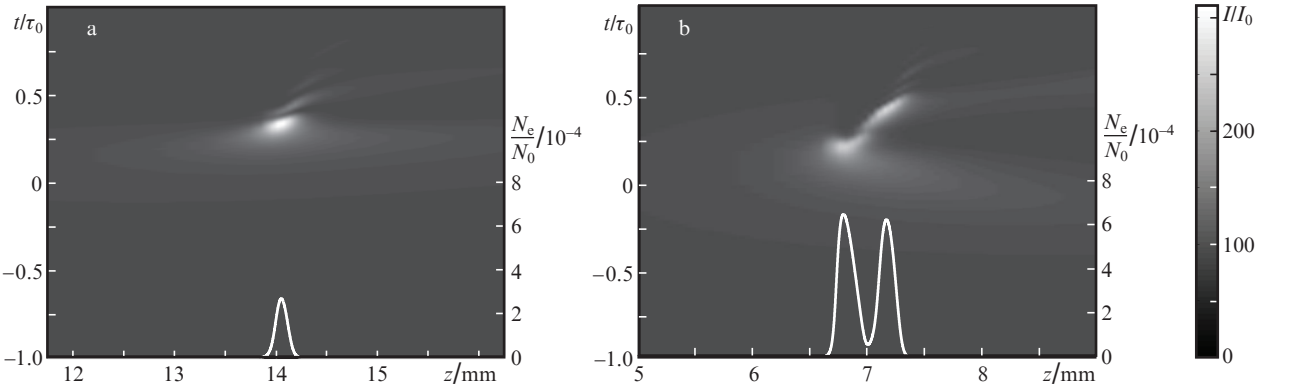

Figure 2. Greyscale presentation of the axial intensity temporal distribution varying with propagation distance $I(r = 0, t, z)$ and the electron concentration profile $N_e(r = 0, z)$ for pulse filamentation in fused silica under the conditions of weak AGVD at $\lambda_0 = 1400$ nm for (a) $W = 0.7$ μJ ($R = 1.2$), $I_0 = 0.18$ TW cm^{-2} and (b) $W = 1.2$ μJ ($R = 2.0$), $I_0 = 0.3$ TW cm^{-2}.

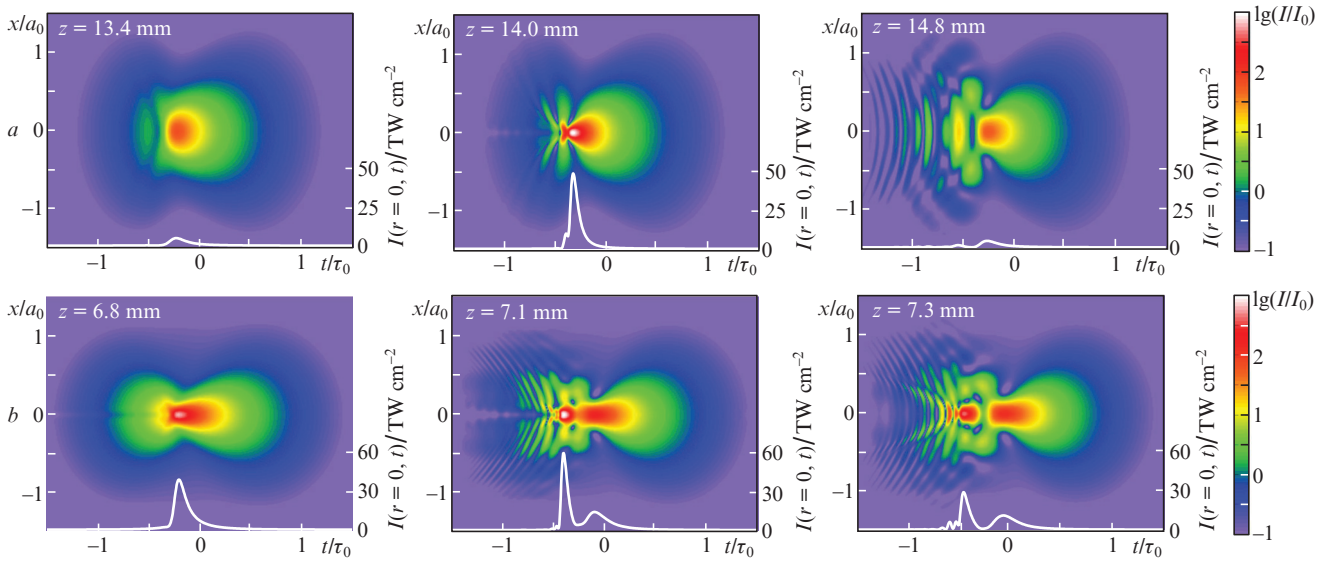

Figure 3. Weak AGVD. Spatiotemporal distributions $I(r,t)$ and profiles of the wave packet axial intensity $I(r = 0,t)$, calculated at a number of characteristic distances in fused silica for the pulse energy (a) $W = 0.7$ μJ ($R = 1.2$) and (b) $W = 1.2$ μJ ($R = 2.0$) ($\lambda_0 = 1400$ nm).

tions of its sharp defocusing in the laser-induced plasma and the effect of the pulse front self-steepening [12].

In the process of pulse propagation in the filament, the length of the plasma channel and, therefore, of the SC generation, is increased, which leads to the broadening of the destructive interference region. As a result, the anti-Stokes wing becomes isolated, its band becomes narrower, and λ_{max}^{as} shifts towards the short-wavelength region (Fig. 4). The growth of the pulse energy W leads to the increase in the plasma channel length (see Fig. 2) and, therefore, to a greater short-wavelength shift of λ_{max}^{as}. Besides that, with increasing W the velocity difference Δv also grows, which, according to the interference model, causes an additional shift of λ_{max}^{as} towards the short-wavelength region [19]. When the pulse energy is increased by two times from 0.7 to 1.4 μJ, the calculated value of λ_{max}^{as} shifts from 725 to 590 nm (see Fig. 1a). The presented analysis explains the experimentally observed shift of the wavelength λ_{max}^{as} of the anti-Stokes band spectral intensity maximum towards the short-wavelength region with increasing W. The values of λ_{max}^{as}, obtained as a result of numerical simulation of filamentation of pulses having different energies in fused silica, are close to those measured in the experiment (Fig. 1a).

In the BaF_2 crystal the filamentation was numerically studied in the case of weak AGVD for the pulses with the centre wavelength $\lambda_0 = 2100$ nm at $\tau_0 = 42$ fs and $a_0 = 46$ μm (Table 1). The variation of the pulse shape and the spectrum of the anti-Stokes SC band in the course of filamentation in BaF_2 is illustrated by Figs 5a and 5b. The peak intensity I_{peak} at the axis of the wave packet achieves its maximal value of 120 TW cm^{-2} at $W = 1.65$ μJ and 135 TW cm^{-2} at $W = 2.1$ μJ (Fig. 5a). With increasing pulse energy the steepness of its trailing edge grows, giving rise to an increase in the anti-Stokes shift of the short-wavelength cut-off, the band of destructive interference broadens, and the short-wavelength shift of the anti-Stokes band maximum grows (Fig. 5b). When W increases from 1.5 μJ ($R = 1.3$) to 2.0 μJ ($R = 1.7$) the wavelength λ_{max}^{as} of the band maximum shifts from 850 to 615 μm (see Fig. 1a).

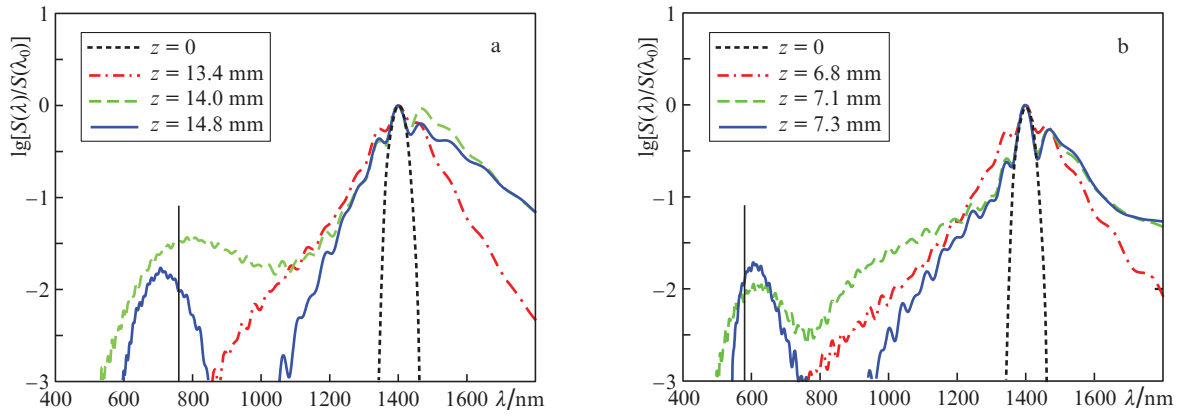

Figure 4. Calculated supercontinuum spectra $\lg[S(\lambda)/S(\lambda_0)]$ at a number of characteristic distances z for filamentation in fused silica under the conditions of weak AGVD at a pulse wavelength $\lambda_0 = 1400$ nm and (a) $W = 0.7$ μJ ($R = 1.2$) and (b) $W = 1.2$ μJ ($R = 2.0$). Vertical lines show the experimentally measured positions of the anti-Stokes band maxima.

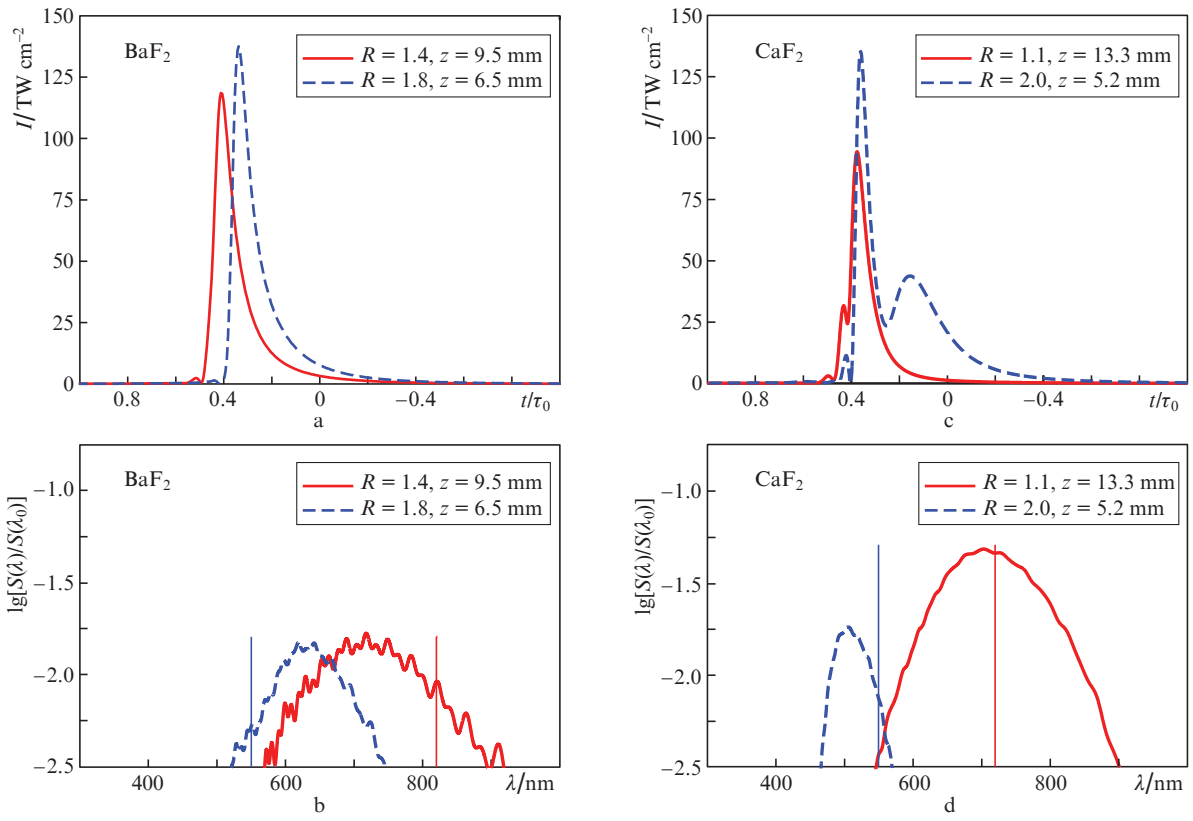

Figure 5. Calculated pulse profiles at a maximum intensity $I(t)$ on the axis of the wave packet in the case of filamentation under conditions of weak AGVD in (a) BaF_2 and (b) CaF_2, as well as spectra in the visible region $\lg[S(\lambda)/S(\lambda_0)]$ in the course of the formation of an isolated anti-Stokes SC wing in (c) BaF_2 and (d) CaF_2. The experimentally measured positions of the anti-Stokes band maximum λ^{as}_{max} are shown by vertical straight lines.

In CaF_2 the weak-AGVD filamentation was numerically studied for the wave packets with the centre wavelength $\lambda_0 = 1800$ nm, $\tau_0 = 42$ fs, and $a_0 = 41$ μm (Table 1). With increasing W the maximal peak intensity I_{peak} increases from 95 to 135 TW cm^{-2}, and the wavelength λ^{as}_{max} shifts from 700 to 500 nm (Figs 5c and 5d). The calculated dependences of λ^{as}_{max} on the pulse energy W for the crystals of BaF_2 and CaF_2 are close to those measured experimentally (see Fig. 1a).

Thus, in the case of weak AGVD in BaF_2 and CaF_2, similar to the case of fused silica, the wavelength λ^{as}_{max} of the spectral intensity maximum of the isolated anti-Stokes band decreases with increasing pulse energy W, as observed in the experiment (Fig. 1a). As follows from the above analysis, this is due to the variation in the group velocity v_b of the compressed wave packet and the extension of the region of destructive interference of SC radiation.

3.2. Strong AGVD

The parameters used for the numerical modelling of strong-AGVD filamentation are summarised in Table 2. Similar to the case of weak AGVD, in this case the peak power P_0 of the pulses insignificantly exceeded P_{cr} at the considered wavelengths in the appropriate materials, but the dispersion length was close to the diffraction length, $L_{dis} \approx L_{dif}$.

Under these conditions, alongside with the compression in the plane perpendicular to the propagation direction, the transformation of the wave packet is accompanied by its compression in time. As a result, a LB with high spatiotemporal localisation of the light field is formed. The variation in the temporal distribution of the intensity $I(r = 0, t, z)$ at the filament axis with distance has the form, characteristic for a LB [7, 8, 15]. As an example, Fig. 6 presents the spatial variations in the axial intensity distributions $I(r = 0, t, z)$ and the electron concentration $N_e(r = 0, z)$ in the laser plasma with distance in the course of filamentation in fused silica and in BaF_2. Due to the spectral shift, the LB group velocity differs from the group velocity of the original wave packet, which leads to its time shift in the accompanying coordinate frame. The direction and velocity of the LB temporal drift essentially depend on the pulse dispersion and the process of dielectric photoionisation [18]. The LB is formed under competing Kerr and plasma nonlinearities, and the variation in I_{peak} and $N_e(r = 0, z)$ with the distance is essentially nonmonotonic (Fig. 6). In the considered pulses after the dissipation of LB in space and time the next LB is formed at a distance of 8 mm in the fused silica and at 6 mm in BaF_2.

Table 2. Parameters of pulses in the case of strong AGVD.

Medium	λ_0/nm	τ_0/fs	a_0/μm	W/μJ	R	L_{dif}/mm	L_{dis}/mm	L_{dis}/L_{dif}
Fused silica	2600	60	72.5	11–13	3.6–4.3	18	12.3	0.7
BaF_2	3800	60	69	7–12	1.3–2.2	11.5	30.7	2.7
CaF_2	3000	60	68	6.8–9.5	1.2–1.6	13.7	41.3	3.0

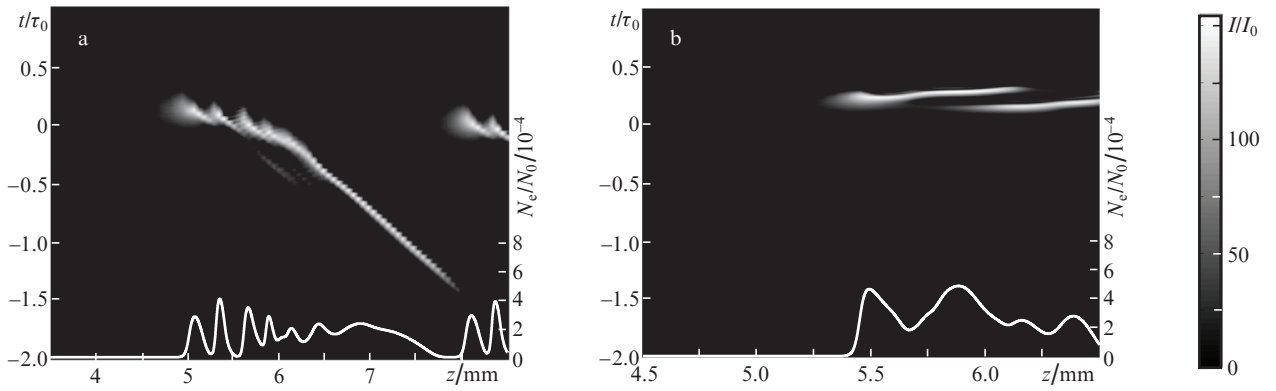

Figure 6. Greyscale patterns of the LB temporal intensity distribution varying with the propagation distance, $I(r = 0, t, z)$, and the electron concentration profiles, $N_e(r = 0, z)$, for pulse filamentation under the conditions of strong AGVD in (a) fused silica at $\lambda_0 = 2600$ nm, $I_0 = 0.63$ TW cm^{-2}, $W = 11$ μJ ($R = 3.6$) and (b) BaF_2 at $\lambda_0 = 3800$ nm, $I_0 = 0.75$TW cm^{-2}, $W = 12$ μJ ($R = 2.2$).

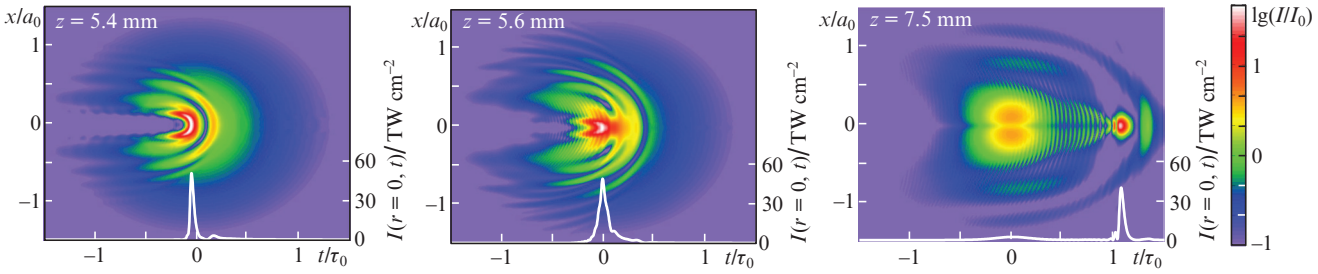

Figure 7. Strong AGVD. Spatiotemporal distributions $I(r, t)$ and profiles of the wave packet axial intensity $I(r = 0, t)$, calculated for a number of characteristic distances in fused silica at $\lambda_0 = 2600$ nm and $W = 11$μJ ($R = 3.6$).

The LB formation is illustrated by Fig. 7, presenting the spatiotemporal distributions of intensity $I(r, t)$ and the axial pulse profiles $I(r = 0, t)$ at a number of characteristic distances z in the course of pulse filamentation at the wavelength 2600 nm in fused silica. One can see that due to plasma defocusing of the LB tail, the intensity distributions in it have the form of a paraboloid, the branches of which are directed towards the pulse tail. The peak intensity in the LB exceeds 50 TW cm^{-2}, its duration is close to the period of optical oscillations, and its diameter varies with the distance, becoming as small as a few wavelengths of the optical radiation. At the distance of 7.5 mm, the LB dissipates, and due to the self-phase modulation, under the conditions of AGVD the next LB is initiated (Fig. 7, right-hand part). This dynamics of a wave packet in the course of the LB formation was obtained in the numerical simulations of pulse filamentation in BaF_2 and CaF_2 at strong AGVD.

The change in the pulse energy by 1.5–2.0 times does not affect the scenario of the LB formation in fused silica, BaF_2, and CaF_2, but increases the number of LBs and their density in the train. The relative offset of the peak intensity in the train does not exceed 1 %. The spectrum of the anti-Stokes SC wing, generated by the LB, the path length of which amounts to 1–3 mm for the considered parameters, is also independent of the pulse energy.

Figure 8 presents the spectra of the SC anti-Stokes wing in fused silica, BaF_2 and CaF_2. According to the numerical simulations, the anti-Stokes wing maximum wavelength is virtually unchanged under the variation in the pulse energy, which agrees with the experimental results (see Fig. 1b). The stability of the parameters and the SC spectrum for the filamentation of pulses having different energies confirms its robustness with respect to the filamentation conditions at strong AGVD.

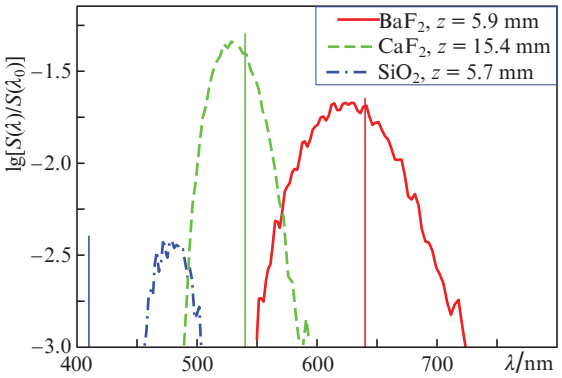

Figure 8. Calculated spectra of the isolated anti-Stokes band in the SC spectrum, lg[$S(\lambda)/S(\lambda_0)$], for strong-AGVD filamentation in fused silica at $\lambda_0 = 2600$ nm, $W = 11$ μJ ($R = 3.6$), in BaF_2 at $\lambda_0 = 3800$ nm, $W = 12$ μJ ($R = 2.2$) and in CaF_2 at $\lambda_0 = 3000$ nm, $W = 6.8$ μJ ($R = 1.2$). The experimentally measured positions of the anti-Stokes band maximum λ^{as}_{max} are shown by vertical straight lines.

4. Similarity parameter for the AGVD 'strength'

The assessment of strong and weak AGVD regions by the magnitude of the dimensioned parameter k_2 does not reflect completely the effect of dispersion on the formation of the LB and related SC spectrum. Indeed, the LB is a result of the light

field self-organisation in the course of its interaction with a nonlinear medium under the AGVD conditions. Its parameters and spectrum are independent of the incident pulse and determined by the wavelength and the medium material dispersion [17, 18]. The LB is formed in the case of consistent self-compression of the wave packet both in time and in space [26]. Before the generation of a laser plasma, the wave packet is compressed due to the phase–amplitude conversion of the light field, the phase shift being caused by the Kerr nonlinearity of the medium. In the second-order approximation of the dispersion theory, valid at the stage of initial compression of the wave packet, the field amplitude $A(r, t, z)$ obeys the equation

$$2ik_0\frac{\partial A}{\partial z} = \Delta_\perp A + k_0|k_2|\frac{\partial^2 A}{\partial t^2} + \frac{2k_0^2}{n_0}\Delta n_{\rm nl}A, \qquad (2)$$

where $\Delta n_{\rm nl} = n_2 I(r, t, z)$ is the increment of the refractive index in the Kerr nonlinear medium. In the dimensionless variables $\zeta = z/L_{\rm dif}$, $\xi = x/a_0$, $\eta = y/a_0$, and $\tau = t/\tau_0$ Eqn (2) takes the form

$$2i\frac{\partial A}{\partial \zeta} = \frac{\partial^2 A}{\partial \xi^2} + \frac{\partial^2 A}{\partial \eta^2} + \frac{L_{\rm dif}}{L_{\rm dis}}\frac{\partial^2 A}{\partial \tau^2} + \frac{2k_0}{n_0}L_{\rm dif}\Delta n_{\rm nl}A. \qquad (3)$$

Provided that $L_{\rm dif}/L_{\rm dis} = 1$, the spatial variables ξ and η in the cross-sectional plane and the time τ are equivalent. This fact means that the self-focusing of the beam and the compression of the pulse occur simultaneously, i.e., the wave packet is compressed in space and time at the same path length in the filament, forming the LB.

If the dispersion length considerably exceeds the diffraction one, $L_{\rm dis} \gg L_{\rm dif}$, then the wave packet has no time to be compressed in time during its spatial self-focusing, and the LB is not formed. The nonlinear refraction in the plasma, induced by the focused beam, gives rise to distortions that disturb the temporal compression and LB formation. This regime of nonlinear optical interaction of the wave packet with the dispersion medium can be identified as filamentation under the conditions of weak AGVD. If $L_{\rm dif} \approx L_{\rm dis}$, then in the pulse, the peak power of which slightly exceeds $P_{\rm cr}$, the stable LBs are formed having a spectrum and parameters, independent of the pulse energy, which can be identified as filamentation under the conditions of strong AGVD. If $L_{\rm dif} \gg L_{\rm dis}$, then the compression of the wave packet in time is faster than its spatial focusing, breaking the concordant spatiotemporal compression. In this case a decrease in the peak intensity of the wave packet, caused by the dispersion pulse broadening at the beginning of propagation before the appearance of essential self-phase modulation in the Kerr medium, can also inhibit the formation of the LB, when the pulse energy decreases [22].

5. Conclusions

The filamentation in transparent dielectrics under the conditions of weak AGVD, when the dispersion length of femtosecond radiation is much greater than its diffraction length, does not lead to the formation of the LB, and the transformation of the spatiotemporal intensity distribution and the spectrum of the wave packet depends on the pulse energy. With an increase in this energy, the peak intensity of the wave packet grows, and due to the broadening of the destructive interference region in the broadband supercontinuum its anti-Stokes wing becomes narrower and shifts towards the short-wavelength region. Under the conditions of strong AGVD, when the dispersion and the diffraction lengths are comparable, the filamentation leads to the formation of a stable LB, the parameters and the spectrum of which are independent of the energy of the incident pulse. Due to this fact, the bandwidth and the position of the intensity maximum in the supercontinuum anti-Stokes wing do not change under the variation of the acting pulse energy.

Acknowledgements. The work was supported the Russian Foundation for Basic Research (Grant Nos 14-22-02025-ofi_m and 15-32-50193-mol_nr), the RF President's Grants Council (State Support to Leading Scientific Schools Programme, Grant No. NSh-9695.2016.2 for) and the Presidium of Russian Academy of Sciences (Programme 'Extreme laser radiation: physics and fundamental applications').

References

1. Couairon A., Mysyrowicz A. *Phys. Rep*., **441**, 47 (2007).
2. Kandidov V.P., Shlenov S.A., Kosareva O.G. *Quantum Electron*., **39**, 205 (2009) [*Kvantovaya Elektron*., **39**, 205 (2009)].
3. Saliminia A., Chin S.L., Vallée R. *Opt. Express*, **13**, 5731 (2005).
4. Naudeau M.L., Law R.J., Luk T.S., Nelson T.R., Cameron S.M., Rudd J.V. *Opt. Express*, **14**, 6194 (2006).
5. Silva F., Austin D.R., Thai A., et al. *Nat. Commun*., **3**, 807 (2012).
6. Jukna V., Galinis J., et al. *Appl. Phys. B*, **116**, 477 (2014).
7. Smetanina E.O., Kompanets V.O., Chekalin S.V., Dormidonov A.E., Kandidov V.P. *Opt. Lett*., **38**, 16 (2013).
8. Durand M., Lim K., Jukna V., McKee E., Baudelet M., Houard A., Richardson M., Mysyrowicz A., Couairon A. *Phys. Rev. A*, **87**, 043820 (2013).
9. Vasa P., Dharmadhikari J.A., Dharmadhikari A.K., Sharma R., Singh M., Mathur D. *Phys. Rev. A*, **89**, 043834 (2014).
10. Dormidonov A.E., Kompanets V.O., Chekalin S.V., Kandidov V.P. *Opt. Express*, **23**, 29202 (2015).
11. Dharmadhikari J.A., Deshpande R.A., Nath A., Dota K., Mathur D., Dharmadhikari A.K. *Appl. Phys. B*, **117**, 471 (2014).
12. Dormidonov A.E., Kandidov V.P. *Laser Phys*., **19**, 1993 (2009).
13. Kolesik M., Wright E.M., Moloney J.V. *Opt. Express*, **13**, 10729 (2005).
14. Smetanina E.O., Kompanets V.O., Dormidonov A.E., Chekalin S.V., Kandidov V.P. *Laser Phys. Lett*., **10**, 10540 (2013).
15. Chekalin S.V., Kompanets V.O., Smetanina E.O., Kandidov V.P. *Quantum Electron*., **43**, 326 (2013) [*Kvantovaya Elektron*., **43**, 326 (2013)].
16. Gražulevičiūtė I., Šuminas R.,Tamošauskas G., Couarion A., Dubietis A. *Opt. Lett*., **40**, 3719 (2015).
17. Chekalin S.V., Kompanets V.O., Dokukina A.E., Dormidonov A.E., Smetanina E.O., Kandidov V.P. *Quantum Electron*., **45**, 401 (2015) [*Kvantovaya Elektron*., **45**, 401 (2015)].
18. Chekalin S., Dokukina A., Dormidonov A., Kompanets V.O., Smetanina E.O., Kandidov V.P. *J. Phys. B: Atomic, Molec. Opt. Phys*., **48**, 094008 (2015).
19. Dormidonov A.E., Kompanets V.O., Chekalin S.V., Kandidov V.P. *Pis'ma Zh. Eksp. Teor. Fiz*., **104**, 173 (2016) [*JETP Lett*., **104**, 175 (2016)].
20. Jiaming Jiang, Yue Zhong, et al. *Phys. Lett. A*, **379**, 1929 (2015).
21. Gražuleviciute I., Garejev N., Majus D., Jukna V., Tamošauskas G., Dubietis A.J. *J. Opt*., **18**, 0255022016 (2016).
22. Zaloznaya E.D., Dormidonov A.E., Kandidov V.P. *Opt. Atmos. Okeana*, **29**, 184 (2016).
23. http://refractiveindex.info.
24. Brabec T., Krausz F. *Phys. Rev. Lett*., **78**, 3282 (1997).
25. Kandidov V.P., Smetanina E.O., Dormidonov A.E., Kompanets V.O. *Zh. Eksp. Teor. Fiz*., **140**, 484 (2011) [*JETP*, **113**, 422 (2011)].
26. Silberberg Y. *Opt. Lett.*, **15**, 1282 (1990).